

# A Stochastic Framework for the Spherical Jeans Equation Motivated by Scalar-Tensor Gravity

Velásquez-Toribio, A. M.<sup>1</sup>

<sup>1</sup>*Center for Astrophysics and Cosmology,*

*Federal University of Espírito Santo, 29075-910 Vitória - ES, Brazil\**

(Dated: June 11, 2026)

We develop a stochastic framework for the stationary spherical Jeans equation, motivated by the field-dependent nature of the gravitational coupling in scalar–tensor theories. We model unresolved spatial fluctuations of the scalar sector as an effective stochastic contribution to the gravitational coupling,  $G_{\text{eff}}(r, \omega) = \bar{G}_{\text{eff}}(r) + \Gamma_G(r)\xi(r, \omega)$ . This approach induces a linear Itô stochastic differential equation for the radial velocity dispersion  $y(r) = \sigma_r^2(r)$ , defining a nonautonomous radial random flow rather than a time-evolution problem. We derive the associated Fokker–Planck equation and obtain integral expressions for the mean, variance, and covariance of the radial velocity dispersion. Because the noise is additive, the deterministic Jeans solution is recovered as the mean profile, while the stochastic sector produces a probability band around it. We specialize the construction to Navarro–Frenk–White, Hernquist, and Einasto halo models and propagate the radial covariance to the projected line-of-sight velocity dispersion. This provides a semi-analytical framework for assessing how effective gravitational fluctuations can affect halo kinematic observables in the stationary Jeans regime.

## I. INTRODUCTION

The spherical Jeans equation is one of the standard tools used to describe the equilibrium dynamics of collisionless self-gravitating systems [1]. It relates the radial velocity dispersion of a tracer population to its density profile, velocity anisotropy, and the gravitational potential. In its usual form, the equation assumes a stationary system, spherical symmetry, and no mean radial streaming motion. These assumptions make it especially useful for the internal regions of relaxed dark-matter halos, elliptical galaxies, galaxy clusters, and dwarf spheroidal galaxies [2].

In the standard application of the Jeans equation, the gravitational coupling is treated as a fixed constant. However, in scalar–tensor theories of gravity the effective gravitational strength is controlled by a scalar field [3–5]. If this scalar field has spatial fluctuations, environmental

---

\* alan.toribio@ufes.br

dependence, or unresolved small-scale variations, the effective gravitational coupling entering the dynamical equation may also fluctuate. The purpose of this work is to formulate a controlled stochastic version of the spherical Jeans equation in which these fluctuations are propagated into the velocity-dispersion profile.

The motivation is twofold. First, scalar–tensor gravity provides a natural setting in which the gravitational coupling is not a rigid parameter but a field-dependent quantity. Second, halo dynamics is often analyzed through deterministic Jeans models even though real systems are affected by substructure, environmental fields, departures from exact equilibrium, and possible modifications of gravity. A stochastic Jeans equation offers a simple way to quantify how such fluctuations broaden the theoretical prediction for the radial and projected velocity dispersions [6–22].

We restrict the present paper to the stationary spherical Jeans regime. This is intentional. The extension to cluster outskirts, where mean radial infall, splashback physics, and the turnaround region become important, requires a generalized Jeans equation with nonzero radial streaming velocity [23–30]. Such a generalization is physically interesting, but it belongs to a different dynamical regime. Here we first construct the simplest analytical framework: a stochastic Jeans equation for the quasi-stationary halo region, together with explicit results for standard halo profiles.

The structure of the paper is as follows. In Sec. II we introduce the scalar–tensor motivation for a stochastic gravitational coupling and derive the stochastic spherical Jeans equation. In Sec. III we obtain the associated Fokker–Planck equation and the probability distribution of the radial velocity dispersion. In Sec. IV we specialize the construction to the Navarro–Frenk–White, Hernquist, and Einasto profiles [31–35]. In Sec. V we present numerical illustrations of the formalism and compare the analytical moment equations with Monte Carlo realizations. Also, Sec. VI summarizes the results and discusses possible extensions to the infall and splashback regions.

## II. STOCHASTIC JEANS EQUATION AND RADIAL RANDOM FLOW

### A. Scalar–tensor motivation for a stochastic gravitational coupling

The motivation for introducing a stochastic gravitational coupling in the Jeans equation comes from a basic property of scalar–tensor gravity: the strength of the gravitational interaction is not necessarily described by a rigid universal constant. Instead, it is controlled by the configuration of an additional scalar degree of freedom. In a broad class of Jordan-frame scalar–tensor theories, the

gravitational sector may be written schematically as

$$S = \frac{1}{16\pi G_*} \int d^4x \sqrt{-g} [F(\phi)R - Z(\phi)g^{\mu\nu}\nabla_\mu\phi\nabla_\nu\phi - 2U(\phi)] + S_m[g_{\mu\nu}, \Psi_m]. \quad (1)$$

Here  $G_*$  denotes a bare gravitational constant,  $g_{\mu\nu}$  is the Jordan-frame metric,  $R$  is the corresponding Ricci scalar, and  $\phi$  is the scalar field. The function  $F(\phi)$  controls the nonminimal coupling between the scalar field and curvature,  $Z(\phi)$  fixes the normalization of the scalar kinetic term, and  $U(\phi)$  is the scalar self-interaction potential. The matter action  $S_m[g_{\mu\nu}, \Psi_m]$  depends on the matter fields  $\Psi_m$  and on the Jordan-frame metric. Therefore, nonrelativistic matter responds to an effective gravitational strength that depends on the scalar configuration.

In the weak-field and quasi-static regime relevant for halo dynamics, the gravitational force entering the Jeans equation can be expressed in terms of an effective gravitational coupling,

$$G_{\text{eff}} = G_{\text{eff}}(\phi, \nabla\phi, \dots). \quad (2)$$

The dots indicate that, depending on the underlying scalar–tensor model and on the approximation scheme,  $G_{\text{eff}}$  may depend not only on the local value of the scalar field but also on its gradients or on quantities associated with screening mechanisms. Thus, even if the Jeans equation is written in an apparently Newtonian form, the coupling multiplying the mass source may carry information about the scalar sector.

We now separate the scalar field into a smooth resolved component and an unresolved fluctuating part,

$$\phi(r, \omega) = \bar{\phi}(r) + \delta\phi(r, \omega). \quad (3)$$

Here  $r$  is the radial coordinate inside the spherical system and  $\omega$  labels a realization of the stochastic scalar configuration. The field  $\bar{\phi}(r)$  represents the coarse-grained scalar profile, whereas  $\delta\phi(r, \omega)$  represents fluctuations around this profile. These fluctuations may effectively encode unresolved small-scale structure, environmental variations, residual departures from perfect equilibrium, or stochastic fluctuations of the scalar sector itself.

Expanding the effective gravitational coupling around the smooth scalar configuration gives, at leading order,

$$G_{\text{eff}}(r, \omega) = G_{\text{eff}}[\bar{\phi}(r)] + \left. \frac{\partial G_{\text{eff}}}{\partial\phi} \right|_{\bar{\phi}} \delta\phi(r, \omega) + \dots. \quad (4)$$

If gradient contributions are relevant, the linear fluctuation may also contain terms of the form

$$\delta G_{\text{eff}}(r, \omega) = \left. \frac{\partial G_{\text{eff}}}{\partial\phi} \right|_{\bar{\phi}} \delta\phi(r, \omega) + \left. \frac{\partial G_{\text{eff}}}{\partial(\nabla_i\phi)} \right|_{\bar{\phi}} \nabla_i\delta\phi(r, \omega) + \dots \quad (5)$$

For the present phenomenological construction, we do not need to specify the microscopic origin of each contribution. We only assume that, after coarse graining, the unresolved scalar-sector fluctuations induce an effective fluctuation in the gravitational coupling. We therefore write

$$G_{\text{eff}}(r, \omega) = \bar{G}_{\text{eff}}(r) + \delta G(r, \omega), \quad (6)$$

where

$$\bar{G}_{\text{eff}}(r) \equiv \langle G_{\text{eff}}(r, \omega) \rangle \quad (7)$$

is the ensemble-averaged, or coarse-grained, effective gravitational coupling. The quantity  $\delta G(r, \omega)$  denotes the stochastic deviation from this mean and is assumed to satisfy

$$\langle \delta G(r, \omega) \rangle = 0. \quad (8)$$

Thus  $\bar{G}_{\text{eff}}(r)$  determines the deterministic Jeans source, whereas  $\delta G(r, \omega)$  describes the unresolved gravitational fluctuation around that mean.

A convenient local representation of this fluctuation is

$$\delta G(r, \omega) = \Gamma_G(r) \xi(r, \omega), \quad (9)$$

so that

$$G_{\text{eff}}(r, \omega) = \bar{G}_{\text{eff}}(r) + \Gamma_G(r) \xi(r, \omega). \quad (10)$$

In this expression,  $\Gamma_G(r)$  controls the radial amplitude of the fluctuation, while  $\xi(r, \omega)$  is a zero-mean stochastic process. The function  $\Gamma_G(r)$  measures how efficiently unresolved scalar-field fluctuations are converted into fluctuations of the gravitational coupling. Schematically, in a perturbative regime one may regard

$$\Gamma_G(r) \xi(r, \omega) \sim \left. \frac{\partial G_{\text{eff}}}{\partial \phi} \right|_{\bar{\phi}} \delta \phi(r, \omega) + \dots, \quad (11)$$

where the ellipsis may include derivative contributions, screening effects, or other coarse-grained corrections.

In the ideal white-noise limit, the stochastic process is represented as

$$\xi(r, \omega) = \frac{dW_r}{dr}, \quad (12)$$

where  $W_r$  is a Wiener process parametrized by the radial coordinate. This expression is only formal:  $dW_r/dr$  is not an ordinary function, but a distributional noise. The corresponding stochastic Jeans equation must therefore be interpreted in the Itô sense. With this normalization, one formally has

$$\langle \xi(r) \rangle = 0, \quad \langle \xi(r) \xi(r') \rangle = \delta(r - r'). \quad (13)$$

Equivalently, the gravitational fluctuation satisfies

$$\langle \delta G(r) \delta G(r') \rangle = \Gamma_G(r) \Gamma_G(r') \delta(r - r') \quad (14)$$

in the white-noise approximation.

A more physical description would use a colored stochastic process with a finite correlation length  $\ell$ ,

$$\langle \delta G(r) \delta G(r') \rangle = \Gamma_G(r) \Gamma_G(r') C_\ell(r, r'), \quad (15)$$

where  $C_\ell(r, r')$  is a correlation kernel. The white-noise model is then recovered when  $C_\ell(r, r')$  becomes sharply peaked around  $r = r'$ . In this sense, the white-noise limit should be understood as an idealized coarse-grained approximation, useful because it leads to a local Fokker–Planck equation and to closed expressions for the mean, variance, and covariance of the Jeans solution.

It is also useful to state the perturbative regime in which the decomposition is physically meaningful. Since  $G_{\text{eff}}$  represents the strength of the attractive gravitational interaction, one should require the stochastic fluctuations to remain small compared with the mean coupling, namely

$$|\delta G(r, \omega)| \ll \bar{G}_{\text{eff}}(r), \quad (16)$$

or, more precisely, that the probability of obtaining negative or unphysically large values of  $G_{\text{eff}}$  is negligible. This assumption ensures that the stochastic model describes small fluctuations around a well-defined mean gravitational interaction.

Thus, if the radial coordinate carries dimensions, the Wiener increment  $dW_r$  has dimensions of  $\sqrt{\text{length}}$ . Therefore, in the white-noise representation, the amplitude  $\Gamma_G(r)$  carries the appropriate units required for  $\Gamma_G(r)dW_r/dr$  to have the same dimensions as a gravitational coupling. If one instead uses the dimensionless coordinate  $x = r/r_s$ , the corresponding normalization factor can be absorbed into a redefined stochastic amplitude. This is the convention adopted below when the stochastic Jeans equation is written in dimensionless form.

## B. Deterministic spherical Jeans equation

We consider a spherically symmetric collisionless system and define

$$y(r) \equiv \sigma_r^2(r), \quad (17)$$

where  $\sigma_r(r)$  is the radial velocity dispersion. The stationary spherical Jeans equation is

$$\frac{dy}{dr} + \left( \frac{d \ln \nu}{dr} + \frac{2\beta}{r} \right) y = -G_{\text{eff}}(r) \frac{M(r)}{r^2}, \quad (18)$$

where  $\nu(r)$  is the tracer density,  $M(r)$  is the enclosed gravitating mass, and

$$\beta(r) = 1 - \frac{\sigma_t^2(r)}{2\sigma_r^2(r)} \quad (19)$$

is the orbital anisotropy parameter. For compactness we define

$$F(r) = \frac{d \ln \nu}{dr} + \frac{2\beta(r)}{r}, \quad H(r) = \frac{M(r)}{r^2}. \quad (20)$$

Then Eq. (18) becomes

$$\frac{dy}{dr} = -F(r)y - G_{\text{eff}}(r)H(r). \quad (21)$$

### C. Stochastic Jeans equation

Using Eq. (10), the Jeans equation becomes a stochastic differential equation along the radial coordinate,

$$dy = [-F(r)y - \bar{G}_{\text{eff}}(r)H(r)] dr - B(r)dW_r, \quad (22)$$

where

$$B(r) = \Gamma_G(r)H(r). \quad (23)$$

The stochastic term is additive because the diffusion coefficient does not depend on the state variable  $y$ . This property makes the model analytically tractable and ensures that, for deterministic boundary data and Gaussian noise, the velocity-dispersion profile is Gaussian distributed.

Equation (22) defines a radial random flow. The radial coordinate plays the role of an evolution parameter, while the stochastic process encodes unresolved scalar-field fluctuations. Since  $F(r)$ ,  $H(r)$ , and  $B(r)$  are explicitly radial-dependent, the corresponding stochastic flow is nonautonomous. Therefore, one should not automatically interpret its probability distribution as a stationary invariant measure. A more appropriate interpretation is that Eq. (22) defines a random radial boundary-value problem, or equivalently a pullback distribution determined by the outer boundary condition.

Let

$$I(r) = \exp \left[ \int^r F(u) du \right] \quad (24)$$

be the deterministic integrating factor. Imposing an outer boundary condition at  $r = r_{\text{out}}$ , the formal solution is

$$y(r) = \frac{I(r_{\text{out}})}{I(r)} y(r_{\text{out}}) + \frac{1}{I(r)} \int_r^{r_{\text{out}}} I(u) \bar{G}_{\text{eff}}(u) H(u) du + \frac{1}{I(r)} \int_r^{r_{\text{out}}} I(u) B(u) dW_u. \quad (25)$$

For the common boundary condition  $y(r_{\text{out}}) = 0$ , the first term vanishes.

### III. FOKKER–PLANCK EQUATION AND RADIAL PROBABILITY DISTRIBUTION

The stochastic Jeans equation derived in the previous section defines a one-dimensional nonautonomous Itô diffusion for the radial velocity-dispersion variable

$$Y_r \equiv y(r) = \sigma_r^2(r). \quad (26)$$

The radial coordinate is not a physical time. Nevertheless, it plays the role of an ordering parameter for the radial boundary-value problem. Accordingly, the probability density  $P(y, r)$  should be interpreted as a radial probability distribution, describing how uncertainties induced by the stochastic gravitational sector are propagated along the halo profile.

The drift and diffusion coefficients associated with Eq. (22) are

$$a(r, y) = -F(r)y - \bar{G}_{\text{eff}}(r)H(r), \quad b(r) = -B(r). \quad (27)$$

Since the diffusion coefficient is independent of  $y$ , the stochastic term is additive. The forward Kolmogorov equation, usually referred to in physics as the Fokker–Planck equation, then gives

$$\frac{\partial P}{\partial r} = \frac{\partial}{\partial y} [(F(r)y + \bar{G}_{\text{eff}}(r)H(r)) P] + \frac{1}{2}B^2(r)\frac{\partial^2 P}{\partial y^2}. \quad (28)$$

The first term represents the deterministic Jeans drift, while the second term describes diffusion in the variable  $y = \sigma_r^2$  generated by the stochastic contribution  $\Gamma_G \xi$  to the effective gravitational coupling.

The local form of Eq. (28) relies on the white-noise coarse-grained limit,  $\xi(r) = dW_r/dr$ . If the fluctuations of the gravitational coupling are modeled as a colored process with finite correlation length, the dynamics is no longer Markovian in  $y$  alone. In that case, the Fokker–Planck description must either be generalized to a nonlocal evolution equation or reformulated in an enlarged state space including the stochastic forcing as an auxiliary variable. In the following, we keep the white-noise limit as the minimal analytically tractable model.

We now use the formal solution obtained in Eq. (25) to compute the statistical moments of the velocity-dispersion profile. Taking the expectation value, and using the fact that the Itô integral has zero mean for an adapted square-integrable integrand, one finds

$$\mathbb{E}[Y_r] = \frac{I(r_{\text{out}})}{I(r)} Y_{r_{\text{out}}} + \frac{1}{I(r)} \int_r^{r_{\text{out}}} I(u) \bar{G}_{\text{eff}}(u) H(u) du. \quad (29)$$

Thus the stochastic mean coincides with the deterministic Jeans solution with the same outer boundary condition. Therefore, in the present additive-noise model, the leading stochastic effect is not a displacement of the mean profile, but the generation of a probability band around it.

The variance is determined by the stochastic integral appearing in Eq. (25). Since the deterministic part does not contribute to the variance, the relevant term is

$$\mathcal{S}(r) = \frac{1}{I(r)} \int_r^{r_{\text{out}}} I(u)B(u)dW_u. \quad (30)$$

Using the Itô isometry,

$$\mathbb{E} \left[ \left( \int_r^{r_{\text{out}}} I(u)B(u)dW_u \right)^2 \right] = \int_r^{r_{\text{out}}} I^2(u)B^2(u)du, \quad (31)$$

we obtain

$$\text{Var}[Y_r] = \frac{1}{I^2(r)} \int_r^{r_{\text{out}}} I^2(u)B^2(u)du. \quad (32)$$

This expression shows explicitly how the fluctuation amplitude  $B(r) = \Gamma_G(r)H(r)$  controls the stochastic broadening of the radial velocity-dispersion profile.

The same argument gives the covariance between the velocity dispersion evaluated at two different radii. The stochastic parts of  $Y_r$  and  $Y_s$  contain Itô integrals over the intervals  $[r, r_{\text{out}}]$  and  $[s, r_{\text{out}}]$ , respectively. Their common stochastic contribution is therefore supported on the overlap interval  $[\max(r, s), r_{\text{out}}]$ . Applying the Itô isometry to this overlap gives

$$\text{Cov}[Y_r, Y_s] = \frac{1}{I(r)I(s)} \int_{\max(r,s)}^{r_{\text{out}}} I^2(u)B^2(u)du. \quad (33)$$

The stochastic Jeans model therefore predicts not only a mean velocity-dispersion profile, but also a radial covariance structure. This covariance is the object that should be propagated when constructing projected observables such as the line-of-sight velocity dispersion.

Because the stochastic Jeans equation is linear and the noise is Gaussian, the solution is Gaussian at each fixed radius whenever the outer boundary value is deterministic. The local probability density can therefore be written as

$$P(y, r) = \frac{1}{\sqrt{2\pi\Sigma^2(r)}} \exp \left[ -\frac{(y - \mu(r))^2}{2\Sigma^2(r)} \right], \quad (34)$$

where

$$\mu(r) = \mathbb{E}[Y_r], \quad \Sigma^2(r) = \text{Var}[Y_r]. \quad (35)$$

The deterministic Jeans model is recovered in the limit  $B(r) \rightarrow 0$ , or equivalently  $\Gamma_G(r) \rightarrow 0$ , in which the probability distribution collapses to a delta distribution centered on the deterministic Jeans solution.

The results obtained in this section are independent of the particular halo profile. All model dependence enters through the functions  $F(r)$ ,  $H(r)$ , the integrating factor  $I(r)$ , and the stochastic amplitude  $B(r) = \Gamma_G(r)H(r)$ . In the next section, these general expressions are specialized to the Navarro–Frenk–White, Hernquist, and Einasto profiles.

#### IV. ANALYTICAL HALO MODELS

In this section we specialize the general stochastic Jeans construction to three standard spherical halo profiles: the Navarro–Frenk–White (NFW), Hernquist, and Einasto models. These examples are useful because they represent different analytical descriptions of halo structure. The NFW profile is the standard benchmark motivated by cosmological  $N$ -body simulations, the Hernquist profile provides a finite-mass model with the same inner cusp as NFW, and the Einasto profile introduces a continuously varying logarithmic slope, allowing one to test the effect of a more flexible halo shape.

We introduce the dimensionless radial coordinate

$$x = \frac{r}{r_s}, \quad (36)$$

where  $r_s$  is the characteristic scale radius of the profile under consideration. For the Einasto profile, we identify this scale with  $r_{-2}$ , the radius at which the logarithmic slope is equal to  $-2$ . For definiteness, we assume in this section that the tracer density  $\nu(r)$  has the same radial dependence as the corresponding halo density profile. This choice keeps the expressions compact and allows us to isolate the effect of the different halo profiles. More generally, one may use a tracer distribution different from the gravitating mass density. In that case, the enclosed mass  $M(r)$  must still be computed from the gravitating profile, while the logarithmic derivative entering the Jeans coefficient must be computed from the tracer density  $\nu(r)$ .

For constant anisotropy parameter  $\beta$ , the dimensionless Jeans equation can be written as

$$\frac{dy}{dx} + \mathcal{F}(x)y = -\bar{\mathcal{A}}(x), \quad (37)$$

where

$$y(x) = \sigma_r^2(x), \quad \mathcal{F}(x) = \frac{d \ln \nu}{dx} + \frac{2\beta}{x}. \quad (38)$$

The deterministic source term is

$$\bar{\mathcal{A}}(x) = \frac{\bar{G}_{\text{eff}}(x)M(x)}{r_s x^2}, \quad (39)$$

whereas the corresponding stochastic amplitude is

$$\mathcal{B}(x) = \frac{\Gamma_G(x)M(x)}{r_s x^2}. \quad (40)$$

Thus  $\bar{\mathcal{A}}(x)$  is the mean gravitational source in the Jeans equation, while  $\mathcal{B}(x)$  controls the amplitude of the random forcing generated by fluctuations of the effective gravitational coupling. If the stochastic equation is written directly in the dimensionless coordinate  $x$ , constant normalization factors associated with the transformation of the Wiener process can be absorbed into the definition of  $\Gamma_G$ .

For any given profile, the integrating factor is

$$I(x) = \exp \left[ \int^x \mathcal{F}(u) du \right]. \quad (41)$$

The general results of Sec. III then give

$$\mu(x) = \frac{1}{I(x)} \int_x^{x_{\text{out}}} I(u) \bar{\mathcal{A}}(u) du, \quad (42)$$

$$\Sigma^2(x) = \frac{1}{I^2(x)} \int_x^{x_{\text{out}}} I^2(u) \mathcal{B}^2(u) du. \quad (43)$$

Here  $x_{\text{out}}$  is the outer boundary at which the radial Jeans problem is closed. Keeping this radius finite is physically natural, since it may represent a virial radius, a splashback radius, an observational aperture, or the scale beyond which the stationary Jeans description is no longer assumed to apply. It is also mathematically useful, especially for profiles whose mass does not converge rapidly at large radius.

### A. Navarro–Frenk–White profile

The Navarro–Frenk–White profile is defined by [31]

$$\rho_{\text{NFW}}(x) = \frac{\rho_s}{x(1+x)^2}. \quad (44)$$

It behaves as  $\rho_{\text{NFW}} \propto x^{-1}$  in the inner region and as  $\rho_{\text{NFW}} \propto x^{-3}$  at large radius. The corresponding enclosed mass is

$$M_{\text{NFW}}(x) = M_s m_{\text{NFW}}(x), \quad m_{\text{NFW}}(x) = \ln(1+x) - \frac{x}{1+x}, \quad (45)$$

where  $M_s = 4\pi\rho_s r_s^3$ . The logarithmic term in  $m_{\text{NFW}}(x)$  implies that the NFW mass grows logarithmically at large radius. Therefore, in a Jeans analysis it is appropriate to impose a finite outer boundary  $x_{\text{out}}$ .

If the tracer density follows the NFW radial dependence, then

$$\frac{d \ln \nu_{\text{NFW}}}{dx} = -\frac{1}{x} - \frac{2}{1+x}. \quad (46)$$

For constant anisotropy, the Jeans coefficient becomes

$$\mathcal{F}_{\text{NFW}}(x) = \frac{2\beta - 1}{x} - \frac{2}{1+x}. \quad (47)$$

The integrating factor is therefore

$$I_{\text{NFW}}(x) = x^{2\beta-1}(1+x)^{-2}, \quad (48)$$

up to an irrelevant multiplicative constant.

The deterministic and stochastic source functions are

$$\bar{\mathcal{A}}_{\text{NFW}}(x) = \frac{\bar{G}_{\text{eff}}(x) M_s m_{\text{NFW}}(x)}{r_s x^2}, \quad (49)$$

$$\mathcal{B}_{\text{NFW}}(x) = \frac{\Gamma_G(x) M_s m_{\text{NFW}}(x)}{r_s x^2}. \quad (50)$$

Consequently, the mean radial velocity dispersion is

$$\mu_{\text{NFW}}(x) = \frac{1}{I_{\text{NFW}}(x)} \int_x^{x_{\text{out}}} I_{\text{NFW}}(u) \bar{\mathcal{A}}_{\text{NFW}}(u) du, \quad (51)$$

and the stochastic variance is

$$\Sigma_{\text{NFW}}^2(x) = \frac{1}{I_{\text{NFW}}^2(x)} \int_x^{x_{\text{out}}} I_{\text{NFW}}^2(u) \mathcal{B}_{\text{NFW}}^2(u) du. \quad (52)$$

These expressions are semi-analytical: the profile dependence is written in terms of elementary functions, and the remaining computation is a one-dimensional quadrature. For special choices of  $\beta$ ,  $\bar{G}_{\text{eff}}(x)$ , and  $\Gamma_G(x)$ , further analytical simplifications may be possible, but the integral representation is the most transparent form for numerical applications and comparisons among profiles.

## B. Hernquist profile

The Hernquist profile is given by [33]

$$\rho_{\text{H}}(x) = \frac{\rho_s}{x(1+x)^3}. \quad (53)$$

It has the same inner cusp as the NFW profile,  $\rho_{\text{H}} \propto x^{-1}$ , but a steeper outer decline,  $\rho_{\text{H}} \propto x^{-4}$ .

As a consequence, its total mass is finite. With a convenient normalization, the enclosed mass is

$$M_{\text{H}}(x) = M_{\text{tot}} \frac{x^2}{(1+x)^2}. \quad (54)$$

This finite-mass property makes the Hernquist model a useful benchmark for testing the stochastic Jeans construction.

For a tracer density proportional to Eq. (53), one obtains

$$\frac{d \ln \nu_{\text{H}}}{dx} = -\frac{1}{x} - \frac{3}{1+x}. \quad (55)$$

Hence

$$\mathcal{F}_{\text{H}}(x) = \frac{2\beta - 1}{x} - \frac{3}{1+x}. \quad (56)$$

The corresponding integrating factor is

$$I_{\text{H}}(x) = x^{2\beta-1}(1+x)^{-3}. \quad (57)$$

The gravitational source takes a particularly simple form because

$$\frac{M_{\text{H}}(x)}{x^2} = \frac{M_{\text{tot}}}{(1+x)^2}. \quad (58)$$

Therefore,

$$\bar{\mathcal{A}}_{\text{H}}(x) = \frac{\bar{G}_{\text{eff}}(x)M_{\text{tot}}}{r_s} \frac{1}{(1+x)^2}, \quad (59)$$

$$\mathcal{B}_{\text{H}}(x) = \frac{\Gamma_G(x)M_{\text{tot}}}{r_s} \frac{1}{(1+x)^2}. \quad (60)$$

The mean and variance are then

$$\mu_{\text{H}}(x) = \frac{1}{I_{\text{H}}(x)} \int_x^{x_{\text{out}}} I_{\text{H}}(u) \bar{\mathcal{A}}_{\text{H}}(u) du, \quad (61)$$

$$\Sigma_{\text{H}}^2(x) = \frac{1}{I_{\text{H}}^2(x)} \int_x^{x_{\text{out}}} I_{\text{H}}^2(u) \mathcal{B}_{\text{H}}^2(u) du. \quad (62)$$

Compared with the NFW case, the Hernquist model has a simpler gravitational source and better asymptotic behavior. For constant  $\bar{G}_{\text{eff}}$  and  $\Gamma_G$ , the kernels entering the mean and variance are rational functions multiplied by the integrating factor. This makes the Hernquist profile especially useful for checking numerical implementations of the stochastic Jeans formalism.

### C. Einasto profile

The Einasto profile is written as [34]

$$\rho_{\text{E}}(x) = \rho_{-2} \exp \left[ -\frac{2}{\alpha_E} (x^{\alpha_E} - 1) \right], \quad (63)$$

where

$$x = \frac{r}{r_{-2}}. \quad (64)$$

Here  $r_{-2}$  is the radius at which the logarithmic slope is equal to  $-2$ , and  $\alpha_E$  controls the curvature of the profile. Unlike the NFW and Hernquist models, the Einasto profile does not have a fixed power-law slope. Instead,

$$\frac{d \ln \rho_E}{d \ln x} = -2x^{\alpha_E}. \quad (65)$$

Thus the logarithmic slope varies continuously with radius, becoming progressively steeper toward the outer halo.

If the tracer density follows the Einasto radial dependence, then

$$\frac{d \ln \nu_E}{dx} = -2x^{\alpha_E-1}. \quad (66)$$

For constant anisotropy,

$$\mathcal{F}_E(x) = -2x^{\alpha_E-1} + \frac{2\beta}{x}. \quad (67)$$

The integrating factor is

$$I_E(x) = x^{2\beta} \exp \left[ -\frac{2}{\alpha_E} x^{\alpha_E} \right], \quad (68)$$

again up to an irrelevant multiplicative constant.

The enclosed mass follows from

$$M_E(x) = 4\pi r_{-2}^3 \int_0^x \rho_E(u) u^2 du. \quad (69)$$

For a general value of  $\alpha_E$ , this integral is not elementary. It can be expressed in terms of the lower incomplete gamma function,

$$\gamma(a, z) = \int_0^z t^{a-1} e^{-t} dt. \quad (70)$$

Using this definition, the enclosed mass is

$$M_E(x) = 4\pi \rho_{-2} r_{-2}^3 e^{2/\alpha_E} \frac{1}{\alpha_E} \left( \frac{\alpha_E}{2} \right)^{3/\alpha_E} \gamma \left( \frac{3}{\alpha_E}, \frac{2x^{\alpha_E}}{\alpha_E} \right). \quad (71)$$

It is also useful to define the total Einasto mass,

$$M_{E,\infty} = 4\pi \rho_{-2} r_{-2}^3 e^{2/\alpha_E} \frac{1}{\alpha_E} \left( \frac{\alpha_E}{2} \right)^{3/\alpha_E} \Gamma \left( \frac{3}{\alpha_E} \right), \quad (72)$$

where  $\Gamma(a)$  is the complete gamma function. Then

$$M_{\text{E}}(x) = M_{\text{E},\infty} m_{\text{E}}(x), \quad (73)$$

with

$$m_{\text{E}}(x) = \frac{\gamma(3/\alpha_{\text{E}}, 2x^{\alpha_{\text{E}}}/\alpha_{\text{E}})}{\Gamma(3/\alpha_{\text{E}})}. \quad (74)$$

The function  $m_{\text{E}}(x)$  is the fraction of the total Einasto mass enclosed within radius  $x$ .

The deterministic source and stochastic amplitude are therefore

$$\bar{\mathcal{A}}_{\text{E}}(x) = \frac{\bar{G}_{\text{eff}}(x)M_{\text{E}}(x)}{r_{-2}x^2}, \quad (75)$$

$$\mathcal{B}_{\text{E}}(x) = \frac{\Gamma_G(x)M_{\text{E}}(x)}{r_{-2}x^2}. \quad (76)$$

The corresponding mean and variance are

$$\mu_{\text{E}}(x) = \frac{1}{I_{\text{E}}(x)} \int_x^{x_{\text{out}}} I_{\text{E}}(u) \bar{\mathcal{A}}_{\text{E}}(u) du, \quad (77)$$

$$\Sigma_{\text{E}}^2(x) = \frac{1}{I_{\text{E}}^2(x)} \int_x^{x_{\text{out}}} I_{\text{E}}^2(u) \mathcal{B}_{\text{E}}^2(u) du. \quad (78)$$

The Einasto case is therefore semi-analytical in a slightly different sense from the NFW and Hernquist cases: the enclosed mass already involves a special function, but once this function is specified, the mean and variance again reduce to one-dimensional quadratures .

#### D. Analytical structure and comparison

The three profiles lead to the same formal stochastic Jeans structure. In each case, the mean profile is obtained from a weighted integral of the deterministic gravitational source  $\bar{\mathcal{A}}(x)$ , while the variance is obtained from a weighted integral of the squared stochastic amplitude  $\mathcal{B}^2(x)$ . The integrating factor  $I(x)$  encodes the combined effect of the tracer logarithmic slope and the anisotropy parameter.

For the NFW and Hernquist profiles, all functions entering the Jeans kernel are elementary. The NFW profile contains a logarithmic mass function and therefore requires a finite outer boundary in practical applications. The Hernquist profile has a finite total mass and a simpler source term, making it a useful benchmark for numerical checks. The Einasto profile has a finite total mass and a curved logarithmic slope, but its enclosed mass involves the lower incomplete gamma function. This is the only special function needed in the present analytical construction.

Once  $\bar{G}_{\text{eff}}(x)$ ,  $\Gamma_G(x)$ ,  $\beta$ , and  $x_{\text{out}}$  are specified, Eqs. (42) and (43) determine the mean radial velocity-dispersion profile and the stochastic probability band for each halo model. These quantities provide the input for the numerical diagnostics discussed in the next section.

### E. Projected line-of-sight velocity dispersion

The radial Jeans solution is connected with observable kinematics through the projected line-of-sight velocity dispersion. For consistency with the finite radial boundary used to close the Jeans problem, we define the projected tracer density as

$$\Sigma_{\text{tr}}(R) = 2 \int_R^{r_{\text{out}}} \frac{\nu(r)r dr}{\sqrt{r^2 - R^2}}. \quad (79)$$

The deterministic projected velocity dispersion is then

$$\sigma_{\text{los,det}}^2(R) = \frac{2}{\Sigma_{\text{tr}}(R)} \int_R^{r_{\text{out}}} \left[ 1 - \beta(r) \frac{R^2}{r^2} \right] \frac{\nu(r)\sigma_r^2(r)r dr}{\sqrt{r^2 - R^2}}. \quad (80)$$

In the stochastic model, the radial quantity  $Y_r = \sigma_r^2(r)$  is a random field with mean  $\mu(r)$  and covariance

$$C_y(r, s) = \text{Cov}[Y_r, Y_s]. \quad (81)$$

It is useful to introduce the projection kernel

$$K(R, r) = \frac{2}{\Sigma_{\text{tr}}(R)} \left[ 1 - \beta(r) \frac{R^2}{r^2} \right] \frac{\nu(r)r}{\sqrt{r^2 - R^2}}. \quad (82)$$

The projected mean is therefore

$$\bar{\sigma}_{\text{los}}^2(R) = \int_R^{r_{\text{out}}} K(R, r)\mu(r) dr. \quad (83)$$

The stochastic uncertainty is propagated through the same projection operator. Hence, the covariance between two projected radii  $R$  and  $R'$  is

$$C_{\text{los}}(R, R') = \int_R^{r_{\text{out}}} dr \int_{R'}^{r_{\text{out}}} ds K(R, r)K(R', s)C_y(r, s). \quad (84)$$

In particular, the variance of the projected line-of-sight dispersion at a fixed projected radius is

$$\text{Var}[\sigma_{\text{los}}^2(R)] = C_{\text{los}}(R, R). \quad (85)$$

This expression shows that the observable uncertainty bands are not inserted phenomenologically, but follow from the radial stochastic Jeans covariance after line-of-sight projection.

## V. SOME NUMERICAL RESULTS

This section should present the main numerical illustrations of the formalism. The purpose is not to perform a full parameter inference, but to show how scalar-field fluctuations propagate into halo kinematic observables. Unless otherwise stated, one may adopt dimensionless units with  $r_s = 1$ ,  $G_0 = 1$ , and a fixed outer radius  $x_{\text{out}}$  sufficiently large for the chosen profile.

Before introducing stochastic effects, it is useful to compare the deterministic ingredients entering the Jeans equation for the three halo models considered in this work. Figure 1 shows the dimensionless density profiles, the enclosed-mass profiles, and the corresponding deterministic radial velocity dispersion obtained from the spherical Jeans equation. The profiles are normalized in a common way in order to isolate differences in shape rather than overall mass scale. The NFW profile provides the standard cosmological benchmark, the Hernquist model has the same inner cusp but a finite total mass, and the Einasto profile displays a continuously varying logarithmic slope. These structural differences propagate directly into the gravitational source term and therefore into the deterministic velocity-dispersion profile.

Figure 2 gives a complementary visualization of the stochastic forcing itself. The lower panel shows the fluctuating gravitational contribution  $\Gamma_G \xi(r)$ , which represents the coarse-grained effect of spatial fluctuations in the scalar sector on the effective gravitational coupling. Positive and negative fluctuations produce local kicks in the radial velocity-dispersion flow. The upper panel shows how these kicks perturb the deterministic Jeans trajectory. The black dashed curve is the deterministic solution obtained when  $\Gamma_G = 0$ , whereas the green curve is one stochastic realization. The thin blue curves represent an ensemble of realizations, illustrating how the stochastic gravitational field broadens the deterministic prediction without necessarily shifting its mean.

The stochastic sector turns the deterministic Jeans solution into a radial probability distribution. Figure 3 shows two complementary diagnostics of this construction. The left panels show local probability densities  $P(y|x)$  at different radii, where  $y = \sigma_r^2$ . Since the noise is additive and Gaussian, each local distribution is Gaussian, with mean and variance determined by the Fokker-Planck solution. The right panels compare the analytical mean and probability bands with Monte Carlo realizations of the radial random flow. The agreement between the Monte Carlo ensemble and the analytical bands verifies that the stochastic broadening is correctly captured by the moment equations derived from the Itô formulation.

The projected line-of-sight velocity dispersion provides the most direct connection between the stochastic Jeans construction and observable halo kinematics. Figure 4 shows  $\sigma_{\text{los}}^2(R)$  for the three

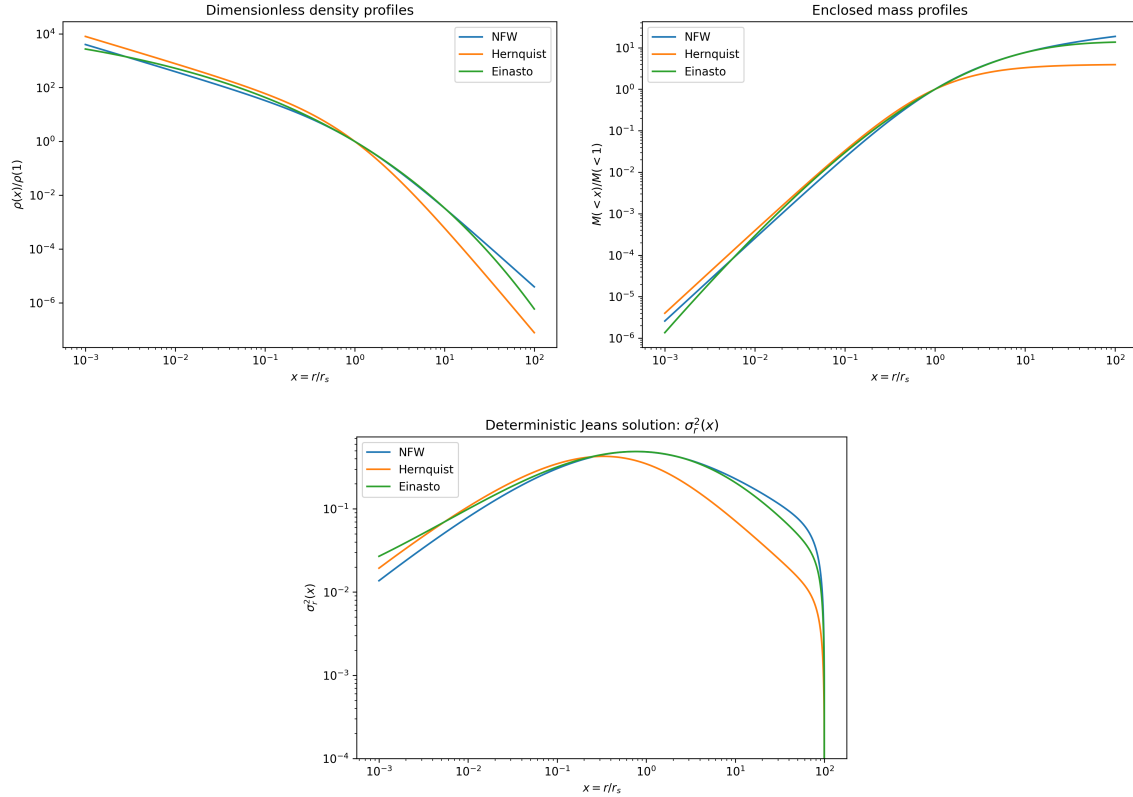


FIG. 1. Dimensionless density, enclosed mass, and deterministic radial velocity-dispersion profiles for the NFW, Hernquist, and Einasto halo models. The density and mass panels display the structural differences between the adopted profiles, while the lower panel shows the corresponding zero-noise Jeans solution for  $\sigma_r^2(x)$  with  $x = r/r_s$ . The NFW profile is used as the cosmological benchmark, the Hernquist model provides a finite-mass analytical comparison, and the Einasto profile represents a curved-slope phenomenological halo model.

halo profiles, including the stochastic uncertainty bands. The projected mean is obtained by inserting the radial mean profile  $\mu(r)$  into the standard projection kernel, whereas the projected variance is computed by propagating the radial covariance through the same kernel. In this way the figure illustrates how fluctuations of the scalar gravitational sector generate observable uncertainty bands in projected kinematic quantities.

A useful way to visualize the stochastic Jeans equation is to regard it as a radial random flow driven from an outer boundary toward smaller radii. Since the coefficients of the stochastic equation depend explicitly on radius, the system is nonautonomous and one should not interpret the limiting probability distribution as a stationary invariant measure in the usual autonomous sense. Instead, the relevant object is a pullback distribution, or equivalently a random attracting graph determined by the outer boundary condition and by the realization of the stochastic forcing.

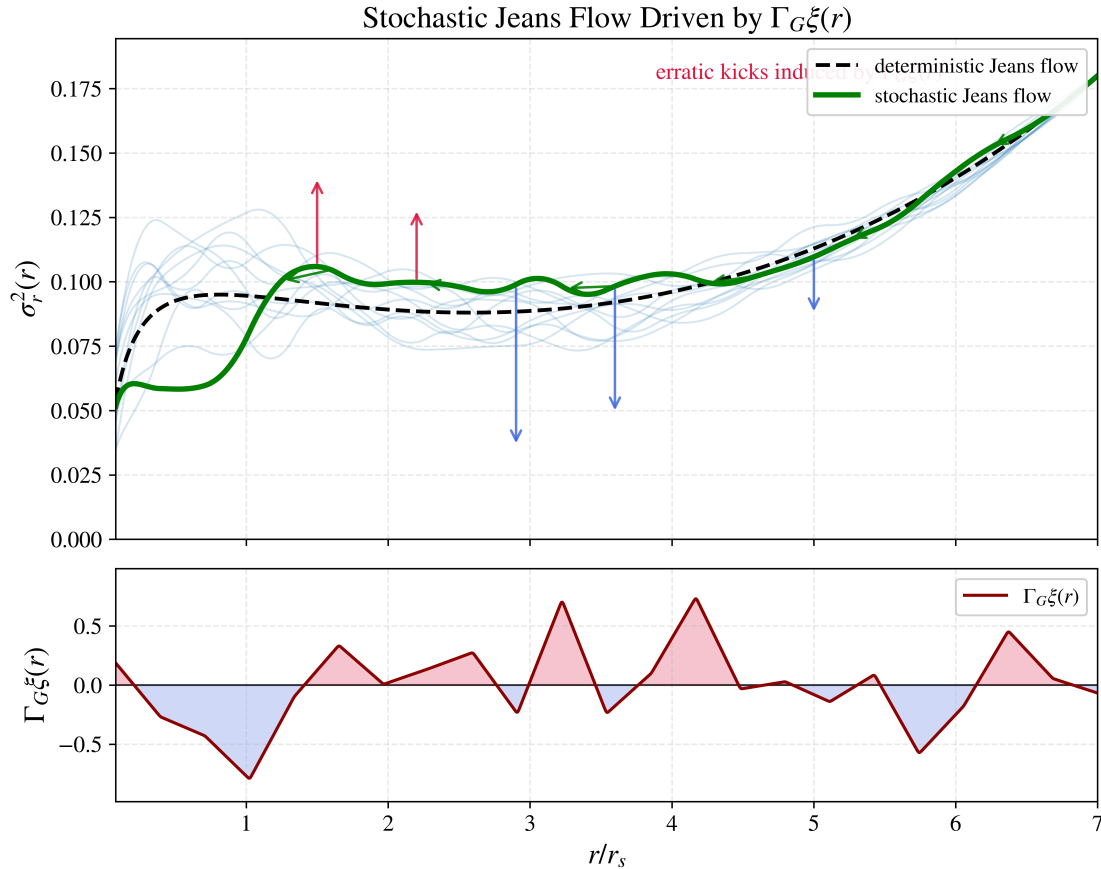


FIG. 2. Stochastic Jeans flow driven by a fluctuating gravitational contribution  $\Gamma_{G\xi}(r)$ . The lower panel shows one realization of the stochastic forcing, with positive and negative regions corresponding to local enhancements or suppressions of the effective gravitational acceleration. The upper panel shows the corresponding effect on  $\sigma_r^2(r)$ : the black dashed curve is the deterministic Jeans solution, the thick green curve is one stochastic realization, and the thin blue curves represent an ensemble of stochastic paths. The vertical arrows indicate local stochastic kicks induced by  $\Gamma_{G\xi}(r)$ . This figure illustrates how scalar-sector fluctuations are propagated into halo kinematics through the stochastic Jeans equation.

Figure 5 illustrates this idea. Several trajectories are initialized with different outer boundary values  $\Delta y_{\text{out}}$  and then evolved inward under the same stochastic radial flow. The rapid convergence of these curves toward the thick green random curve shows the loss of memory of the imposed external boundary data. In this operational sense, the green curve represents the pullback attractor of the stochastic Jeans flow: it is the limiting random profile selected by the dynamics when the boundary data are propagated inward. This should not be confused with a fixed point in phase space; it is a random radial profile, or random graph, associated with the nonautonomous stochastic boundary-value problem.

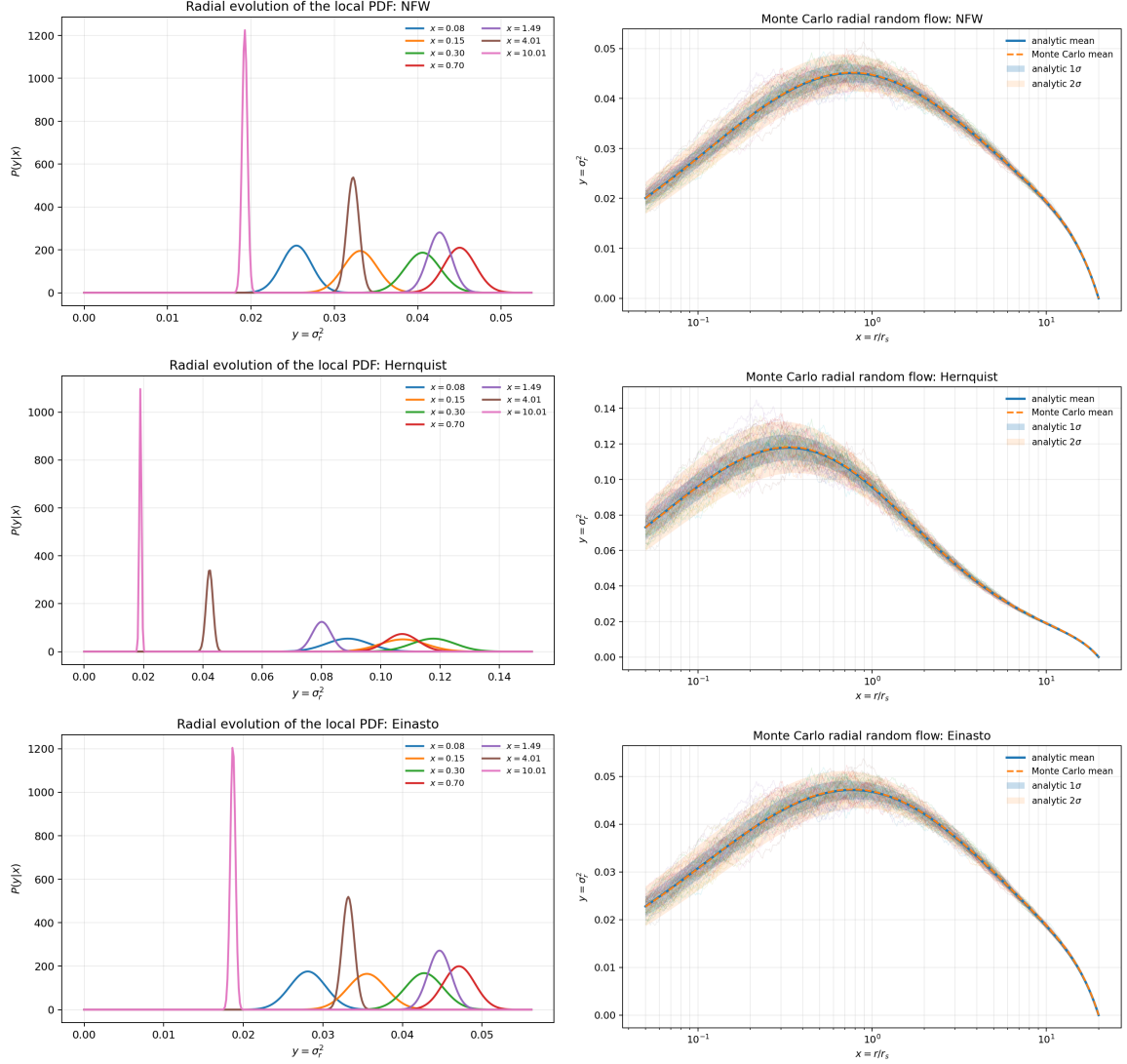


FIG. 3. Radial probability distribution and Monte Carlo realization of the stochastic Jeans flow for the NFW, Hernquist, and Einasto profiles. Left panels: local probability densities  $P(y|x)$  for  $y = \sigma_r^2$  at selected radii. The displacement and narrowing or broadening of the distributions reflect the radial dependence of the mean and variance obtained from the Fokker–Planck equation. Right panels: Monte Carlo realizations of the radial random flow compared with the analytical mean and the  $1\sigma$  and  $2\sigma$  probability bands. The stochastic mean coincides with the deterministic Jeans solution, while the variance quantifies the broadening induced by fluctuations in the effective gravitational coupling.

### A. Validity regime and possible extension to infall

The present framework applies to the stationary spherical Jeans regime. It is therefore most appropriate for the quasi-virialized region of halos, where mean radial streaming velocities are negligible compared with random motions. In the outskirts of galaxy clusters, especially between the

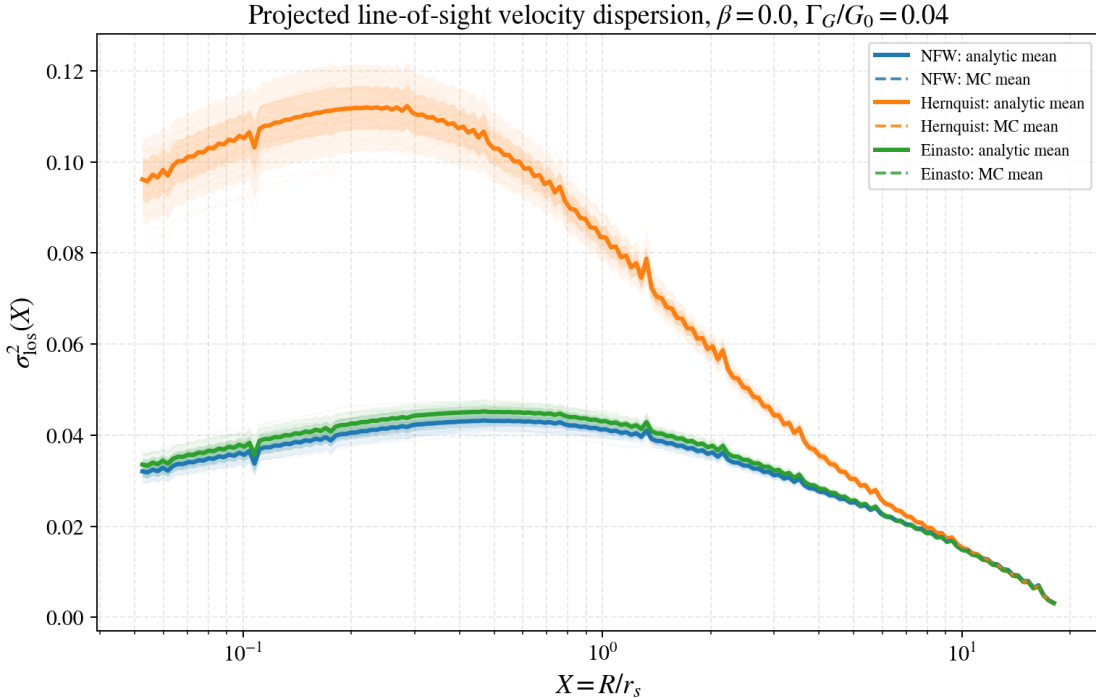


FIG. 4. Projected line-of-sight velocity dispersion for the NFW, Hernquist, and Einasto profiles. Solid curves show the analytical projected mean, shaded regions show the stochastic uncertainty bands, and dashed curves show the Monte Carlo projected means. The bands are obtained by propagating the radial covariance of  $\sigma_r^2$  through the line-of-sight projection kernel.

virial radius, the splashback radius, and the turnaround radius, radial infall becomes dynamically important. In that regime the generalized Jeans equation contains an additional streaming term of the form

$$\bar{v}_r \frac{\partial \bar{v}_r}{\partial r} + \frac{\partial \bar{v}_r}{\partial t}, \quad (86)$$

where  $\bar{v}_r$  is the mean radial velocity. A stochastic extension of that generalized equation is a natural continuation of the present work, but it should be treated separately because it describes a nonstationary region of halo dynamics.

Taken together, these figures show that the stochastic Jeans equation provides a controlled way to propagate fluctuations of the effective gravitational coupling into halo kinematic observables. At the radial level, the stochastic sector generates a probability distribution for  $\sigma_r^2(r)$  rather than a single deterministic profile. At the projected level, the same covariance structure produces uncertainty bands for  $\sigma_{\text{los}}^2(R)$ , which are directly connected with observational velocity-dispersion measurements. The pullback-attractor visualization further clarifies the role of the outer boundary condition: for a fixed stochastic realization, different imposed boundary data may converge toward

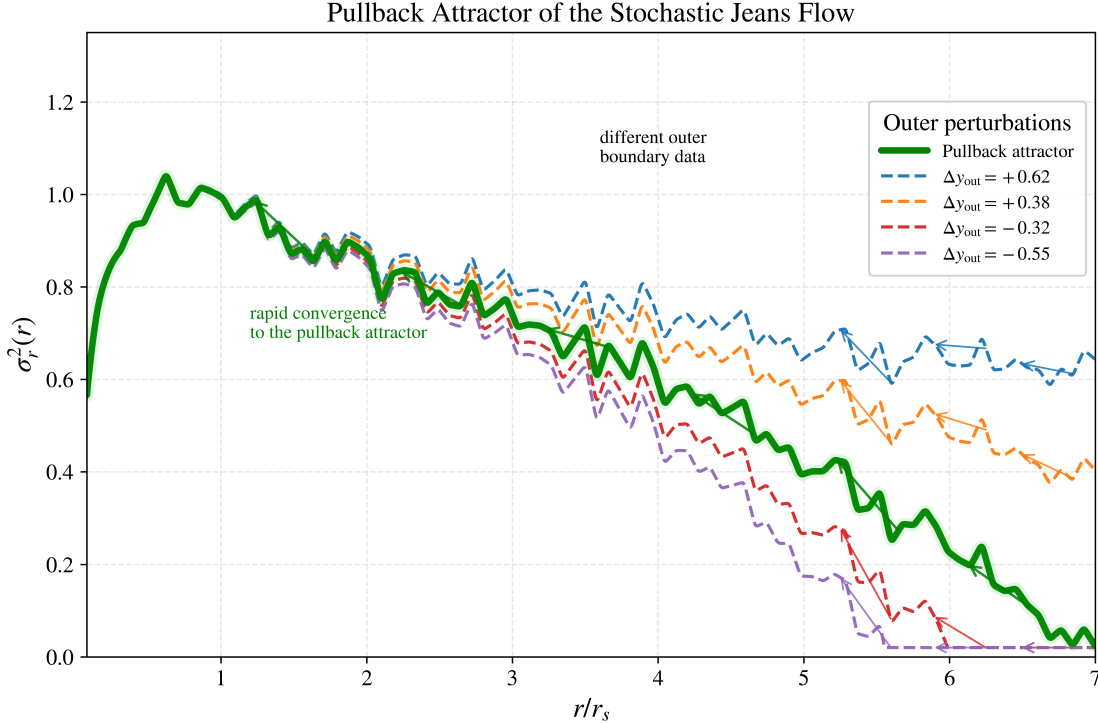


FIG. 5. Pullback attractor of the stochastic Jeans flow. The dashed curves represent solutions initialized at the outer boundary with different values of  $\Delta y_{\text{out}}$ , while the thick green curve represents the limiting random profile selected by the stochastic radial flow. The arrows indicate inward evolution from large to small radii. The convergence of different boundary-data realizations toward the same random curve illustrates the pullback character of the solution: the system loses memory of the imposed outer boundary condition and approaches a stochastic attracting profile for  $y(r) = \sigma_r^2(r)$ . Because the radial flow is nonautonomous, this object should be interpreted as a pullback attractor or random attracting graph, not as a stationary fixed point.

the same limiting random profile, showing that the stochastic radial flow can select an effective attracting solution.

## VI. CONCLUSIONS

We have formulated a stochastic extension of the stationary spherical Jeans equation motivated by scalar–tensor gravity. In this framework, fluctuations of the scalar sector induce fluctuations in the effective gravitational coupling, which are represented after coarse graining as  $G_{\text{eff}}(r, \omega) = \bar{G}_{\text{eff}}(r) + \Gamma_G(r)\xi(r, \omega)$ . This leads to a linear Itô stochastic differential equation for  $y(r) = \sigma_r^2(r)$  along the radial coordinate.

The radial coordinate is not a physical time, but it acts as an ordering parameter for the Jeans boundary-value problem. The stochastic Jeans equation therefore defines a nonautonomous radial random flow. In the white-noise limit, the associated Fokker–Planck equation gives the radial probability distribution  $P(y, r)$ . Because the noise is additive, the deterministic Jeans solution is recovered as the mean profile, while the stochastic sector generates a probability band around it. We derived closed integral expressions for the variance and covariance of  $\sigma_r^2(r)$  using the Itô isometry.

The formalism was applied to NFW, Hernquist, and Einasto halo models. For NFW and Hernquist profiles, the relevant kernels are written in terms of elementary functions, while the Einasto enclosed mass involves the lower incomplete gamma function. In all cases, the stochastic mean, variance, and covariance reduce to one-dimensional quadratures once the profile, anisotropy, mean coupling, fluctuation amplitude, and outer boundary are specified.

The numerical examples illustrate how stochastic fluctuations of the effective gravitational coupling propagate into halo kinematic observables. At the radial level, the model predicts a probability distribution for  $\sigma_r^2(r)$ . At the projected level, the radial covariance produces uncertainty bands for the line-of-sight velocity dispersion  $\sigma_{\text{los}}^2(R)$ . Monte Carlo realizations of the radial random flow agree with the analytical moment equations, providing a direct consistency check of the Fokker–Planck formulation.

We also emphasized the pullback interpretation of the stochastic Jeans flow. Since the system is nonautonomous in radius, the limiting random profile should be understood as a pullback attracting graph selected by the inward propagation from the outer boundary, rather than as a stationary invariant measure. This interpretation clarifies how different outer boundary perturbations can lose memory of their initial values and approach a common stochastic profile.

The present work is restricted to the stationary spherical Jeans regime. Applications to cluster outskirts, splashback, or turnaround regions require a generalized Jeans equation with mean radial streaming and possible explicit time dependence. These extensions will be important for connecting the present stochastic framework with nonstationary halo dynamics and will be pursued in future work.

## ACKNOWLEDGMENTS

I would like to thank Maria Margarita and Miguel Amado for their continuous inspiration and support, and the Foundation for Research Support of Espírito Santo (FAPES) for the partial support

for the present work.

- 
- [1] J. H. Jeans, “On the theory of star-streaming and the structure of the universe,” *Mon. Not. Roy. Astron. Soc.* **76**, 70 (1915).
  - [2] J. Binney and S. Tremaine, *Galactic Dynamics*, 2nd ed. (Princeton University Press, Princeton, 2008).
  - [3] C. Brans and R. H. Dicke, “Mach’s principle and a relativistic theory of gravitation,” *Phys. Rev.* **124**, 925 (1961).
  - [4] T. Clifton, P. G. Ferreira, A. Padilla, and C. Skordis, “Modified gravity and cosmology,” *Phys. Rept.* **513**, 1 (2012).
  - [5] A. De Felice and S. Tsujikawa, “f(R) theories,” *Living Rev. Rel.* **13**, 3 (2010).
  - [6] L. Arnold, *Random Dynamical Systems* (Springer, Berlin, 1998).
  - [7] B. Øksendal, *Stochastic Differential Equations: An Introduction with Applications* (Springer, Berlin, 2003).
  - [8] A. Kolmogoroff, “Über die analytischen Methoden in der Wahrscheinlichkeitsrechnung,” *Math. Ann.* **104**, 415–458 (1931).
  - [9] K. Itô, “Stochastic integral,” *Proc. Imp. Acad. Tokyo* **20**, 519–524 (1944).
  - [10] R. Khasminskii, *Stochastic Stability of Differential Equations*, 2nd ed. (Springer, Berlin, 2012).
  - [11] H. Kunita, *Stochastic Flows and Stochastic Differential Equations* (Cambridge University Press, Cambridge, 1990).
  - [12] H. Crauel and F. Flandoli, “Attractors for random dynamical systems,” *Probab. Theory Relat. Fields* **100**, 365–393 (1994).
  - [13] H. Crauel, A. Debussche, and F. Flandoli, “Random attractors,” *J. Dyn. Differ. Equ.* **9**, 307–341 (1997).
  - [14] P. E. Kloeden and M. Rasmussen, *Nonautonomous Dynamical Systems* (American Mathematical Society, Providence, 2011).
  - [15] S. Chandrasekhar, “Stochastic problems in physics and astronomy,” *Rev. Mod. Phys.* **15**, 1–89 (1943).
  - [16] H. E. Kandrup, “Stochastic gravitational fluctuations in a self-consistent mean field theory,” *Phys. Rep.* **63**, 1–59 (1980).
  - [17] E. L. Łokas and G. A. Mamon, “Dark matter distribution in the Coma cluster from galaxy kinematics: breaking the mass–anisotropy degeneracy,” *Mon. Not. Roy. Astron. Soc.* **343**, 401–412 (2003).
  - [18] G. A. Mamon and E. L. Łokas, “Dark matter in elliptical galaxies. II. Estimating the mass within the virial radius,” *Mon. Not. Roy. Astron. Soc.* **363**, 705–722 (2005).
  - [19] G. A. Mamon, A. Biviano, and G. Boué, “MAMPOSSt: Modelling anisotropy and mass profiles of observed spherical systems. I. Gaussian 3D velocities,” *Mon. Not. Roy. Astron. Soc.* **429**, 3079–3098 (2013).

- [20] L. Lombriser, F. Schmidt, T. Baldauf, R. Mandelbaum, U. Seljak, and R. E. Smith, “Cluster density profiles as a test of modified gravity,” *Phys. Rev. D* **85**, 102001 (2012).
- [21] L. Lombriser, K. Koyama, G.-B. Zhao, and B. Li, “Chameleon  $f(R)$  gravity in the virialized cluster,” *Phys. Rev. D* **85**, 124054 (2012).
- [22] C. Escudero and C. Manada, “Itô versus Stratonovich in a stochastic cosmological model,” *Lett. Math. Phys.* **112**, 12 (2022).
- [23] M. Falco, S. Hansen, R. Wojtak, G. A. Mamon, and A. V. Maccio, “Dynamical signatures of infall around galaxy clusters,” *Mon. Not. Roy. Astron. Soc.* **431**, L6 (2013).
- [24] S. More, B. Diemer, and A. V. Kravtsov, “The splashback radius as a physical halo boundary and the growth of halo mass,” *Astrophys. J.* **810**, 36 (2015).
- [25] B. Bar-Or, J.-B. Fouvry, and S. Tremaine, “Relaxation in a fuzzy dark matter halo. II. Self-consistent kinetic equations,” *Astrophys. J.* **915**, 27 (2021).
- [26] B. T. Chiang, J. P. Ostriker, and H.-Y. Schive, “Can ultralight dark matter explain the age–velocity dispersion relation of the Milky Way disc: A revised and improved treatment,” *Mon. Not. Roy. Astron. Soc.* **518**, 4045–4063 (2023).
- [27] H.-Y. Yang, et al., “Galactic disc heating by density granulation in fuzzy dark matter simulations,” *Mon. Not. Roy. Astron. Soc.* **530**, 129–148 (2024).
- [28] N. Dalal and A. Kravtsov, “Heating of Galactic Disks by Diffuse Dark Matter Substructure,” *Astrophys. J.* **908**, 24 (2021).
- [29] D. Dutta Chowdhury, F. C. van den Bosch, and H.-Y. Schive, “The dynamical effects of fuzzy dark matter fluctuations on the orbit of the Sagittarius stream,” *Mon. Not. Roy. Astron. Soc.* **521**, 1045–1061 (2023).
- [30] H. N. Luu, B. McKague, and C. P. Hayden, “Constraints on ultralight dark matter from the vertical heating of the Milky Way disc,” *Phys. Rev. D* **110**, 083512 (2024).
- [31] J. F. Navarro, C. S. Frenk, and S. D. M. White, “The structure of cold dark matter halos,” *Astrophys. J.* **462**, 563 (1996).
- [32] J. F. Navarro, C. S. Frenk, and S. D. M. White, “A universal density profile from hierarchical clustering,” *Astrophys. J.* **490**, 493 (1997).
- [33] L. Hernquist, “An analytical model for spherical galaxies and bulges,” *Astrophys. J.* **356**, 359 (1990).
- [34] J. Einasto, “On the construction of a composite model for the Galaxy and on the determination of the system of Galactic parameters,” *Trudy Astrofiz. Inst. Alma-Ata* **5**, 87 (1965).
- [35] D. Merritt, A. W. Graham, B. Moore, J. Diemand, and B. Terzić, “Empirical models for dark matter halos. I. Nonparametric construction of density profiles and comparison with parametric models,” *Astron. J.* **132**, 2685 (2006).